Journal of Advanced Marine Engineering and Technology, Vol. 50, No. 1, pp. 43~50, 2026
J. Advanced Marine Engineering and Technology (JAMET)
https://doi.org/10.5916/jamet.2026.50.1.43

ISSN 2234-7925 (Print)
ISSN 2765-4796 (Online)
Original Paper

Verification of the initial design of a high-head two-stage centrifugal pump on the performance and structural stability by numerical analysis

Eshan Fernando[1] · Ujjwal Shrestha[2] · Daehoon Kim[3] · Young-Do Choi†

(Received November 10, 2025 ; Revised November 23, 2025 ; Accepted February 8, 2026)

Abstract: Application of a submerged two-stage centrifugal pump is a unique concept to pump water to a higher elevation. This pump contains a long vertical shaft, which is responsible for the impeller rotation. The impellers of the pump are arranged in an opposite direction, and the crossover guides the flow from 1st stage to 2nd stage impellers. In order to verify the acceptability of the initial design of a high-head two-stage centrifugal pump, numerical analysis is performed to evaluate the pump performance, internal flow characteristics, and the structural stability of the long shaft, which is more prone to vibrations. The calculations were done in the range of flow rates to check the pump operation in partial and excessive flow rates. Results revealed that the pump shaft has very low vibrations, indicating the structural stability with a relatively large margin below the ultimate tensile stress.

Keywords: Submerged high-head two-stage centrifugal pump, Long vertical shaft, Numerical analysis, Hydraulic performance, Structural stability

1. Introduction

A multistage centrifugal pump is used for industrial applications with high head requirements. Multistage centrifugal pumps, including two-stage designs, are engineered to achieve a higher head than single-stage pumps by arranging multiple impellers in series along the pump shaft **[1]**. These types of multistage pumps may face structural failure due to the high hydraulic pressure that they generate, which places a substantial load on impellers and connecting components. Ding et al. utilized numerical simulations to characterize multistage pump performance under varying operating conditions **[2]**. The computational fluid dynamics (CFD) approach can be used to perform the internal flow and loss analysis of the centrifugal pump to determine the pump characteristics **[3][4]**. Shebin Yan *et al.* used a fluid structure interaction (FSI) approach to analyze the structural integrity of a high-speed centrifugal pump rotor system **[5]**. Leta Yadeta *et al.* performed a numerical fatigue stress analysis on a multistage centrifugal pump shaft, indicating the difference in stress acting on the pump shaft in varying flow conditions **[6].** Bob Mischo and Albadawi analyzed a high-head and ultra-high-speed centrifugal pump, where the Fluid-Structure Interaction (FSI) analysis is essential for validating mechanical integrity **[7][8].** Zhou et al. also performed a fluid-structure interactions approach to investigate the rotodynamic characteristics of a centrifugal pump **[9]**.

The use of a two-stage centrifugal pump as a submerged pump for a high-head application is a unique approach adopted for an industrial purpose. Therefore, this research focuses on the numerical modelling of the acceptability of the initial design of the high-head two-stage submerged centrifugal pump, which can serve as a preliminary analysis of the design before physical testing.

2. 3D Modeling of The Pump

2.1 Design Specification of the Model

The two-stage centrifugal pump was designed for an industrial application that requires a high head value and a comparatively low flow rate. The rotational speed of the pump is 1731 min^{-1}. Due to high head and low flow, the resulting specific speed exhibits a relatively low value**.** This low specific speed indicates the pump's hydraulic geometry is the radial flow type, which is optimally suited for high head applications. **Table 1** lists all essential pump specifications and their corresponding values.

† Corresponding Author (ORCID: https://orcid.org/0000-0001-7316-1153): Professor, Department of Mechanical Engineering, Institute of New and Renewable Energy Technology Research, Mokpo National University, 1666 Youngsan-ro, Cheonggye-myeon, Muan-gun, Jeonnam, 58554, Korea, E-mail: ydchoi@mnu.ac.kr, Tel: 061-450-2419
1 M. S., Department of Mechanical Engineering, Mokpo National University, E-mail: 25141304@mokpo.ac.kr
2 Researcher, Institute of New and Renewable Energy Technology Research, Mokpo National University, E-mail: ujjwal10@mnu.ac.kr
3 NS Hydro Co. Ltd, E-mail: kimspump@gmail.com

Table 1: Design specifications of the pump

Parameter	Value
Head (*H*)	158 [m]
Flow rate (*Q*)	10.39 [m^3/min]
`Rotational speed (*N*)	1731 [min^{-1}]
*Specific speed(n_s)	125 [min^{-1},m^3/min ,m]

2.2 3D Modeling of a Two-Stage Submerged Centrifugal Pump

The 3D model of the two-stage submerged centrifugal pump was developed based on the design specifications given in **Table 1**. As this pump is a low-specific-speed pump, it is suitable for high-head, low-flow applications. The 3D geometry was modeled by ANSYS SpaceClaim 2025 R1 **[10]** and is shown in **Figure 1**. The 3D cross-sectional views indicate the material within the pump structure. The resulting solid model will act as the reference geometry for the Fluid-Structure Interaction (FSI) simulations of the pump assembly.

Figure 2 illustrates a cross-sectional schematic view of the fluid domain extracted from the structural domain of the two-stage centrifugal pump model. In the extracted fluid domain, geometric features were preserved adequately alongside gap clearances between impellers and casing, which is important for the accurate determination of pressure variation and efficiency calculation.

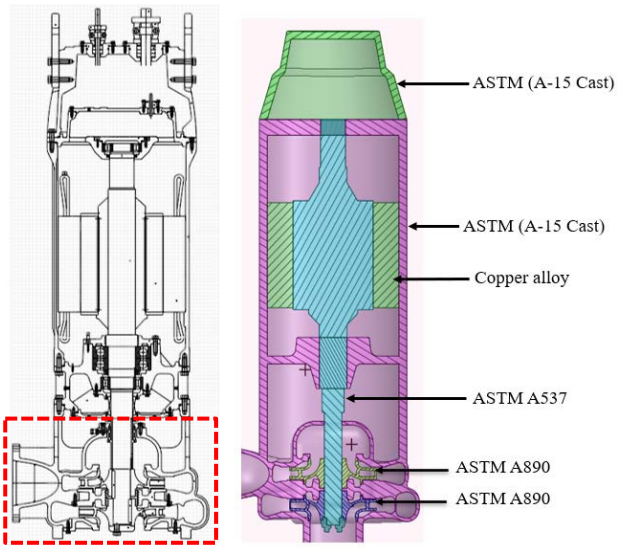

Figure 1: Cross-sectional view of the pump 2D drawing (left) and 3D structural domain for FSI analysis (right)

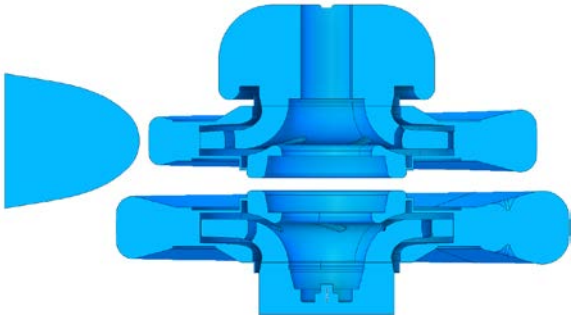

Figure 2: Fluid domain of a two-stage centrifugal pump model for CFD analysis, as indicated by the dotted red box in **Figure 1**

3. Numerical Methodology

3.1 Numerical Mesh and Boundary Conditions for CFD Analysis

The extracted fluid volumes in **Figure 2** are sectioned into six parts to compute the numerical grids of each section. Each fluid component was meshed with numerical grids to capture the flow characteristics of the pump. The numerical grids of the two-stage centrifugal pump model parts are shown in **Figure 3**, and the grid element numbers are shown in **Table 2**. A tetrahedral mesh was used for the geometry of the two-stage centrifugal pump.

The numerical grids for the impeller, casing, and other parts are generated using ANSYS meshing **[10].**

Table 2: Numerical grids element numbers of each part

Part name	No of elements
1st stage impeller	1.1×10^5
2nd stage impeller	1.1×10^5
Casing	26.5×10^5
Cross over	6.8×10^5
Total	35.5×10^5

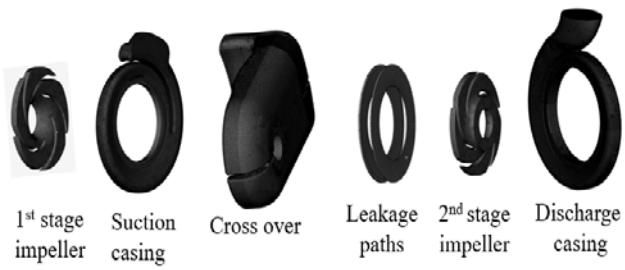

Figure 3: Numerical grids of the pump model parts for the CFD analysis

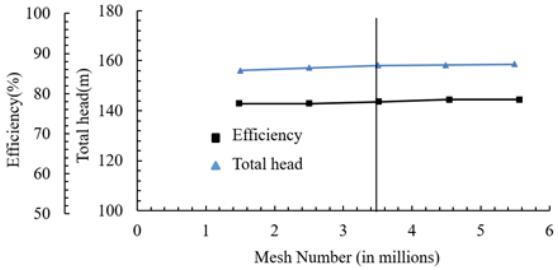

Figure 4: Results of the grid dependency test of the two-stage centrifugal pump model at Q/Q_{BEP} = 1.0.

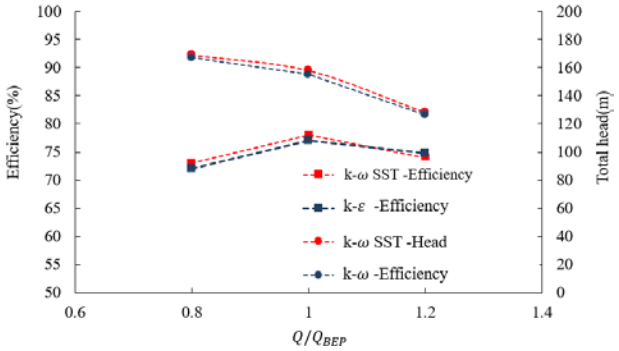

Figure 5: Turbulence model dependency test of the two-stage centrifugal pump model at a) Q/Q_{BEP} = 0.8, b) Q/Q_{BEP} = 1.0, and c) Q/Q_{BEP} = 1.0.

Table 3: Boundary conditions for CFD analysis

Parameter	Conditions/Value
Analysis type	Steady state
Inlet	Static pressure
Outlet	Mass flow rate
Rotational speed	1731 min^{-1}
Turbulence model	k-ω SST
Interface model	Frozen rotor

The grid dependency test, shown in **Figure 4,** was performed to investigate the influence of the grid number on the computational results. The mesh element number of 3.55 million was selected for the entire pump model domain analysis. **Figure 5** illustrates the turbulence model dependency test performed on this mesh. It shows a maximum variation of only 1.9% in the head and 1.2% in the efficiency across k-ω and k-ω SST turbulence models.

The detailed boundary conditions for the CFD analysis are shown in **Table 2**. The shear stress turbulence model is selected for the numerical calculation because it shows better convergence for the rotating fluid machinery. The inlet and outlet boundary conditions were static pressure and mass flow rate, respectively. The frozen rotor was selected as the interface model between the stationary and rotating components **[11][12].**

3.2 FSI Numerical Methodology

Tang *et al.* demonstrated the application of one-way FSI analysis for assessing the structural integrity of a turbomachine impeller **[13]**. In the present study, a unidirectional coupling approach was employed to analyze the structural response of the centrifugal pump under the influence of fluid pressure. **Figure 6** shows the tetrahedral numerical grid created for the 1st and 2nd stage impellers, pump shaft, and motor rotor created using the ANSYS meshing **[14]**. This numerical grid was used for the FSI (Fluid-Structural Interaction) analysis.

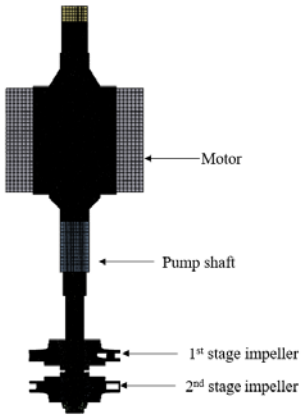

Figure 6: Numerical grids of the pump model for the FSI analysis

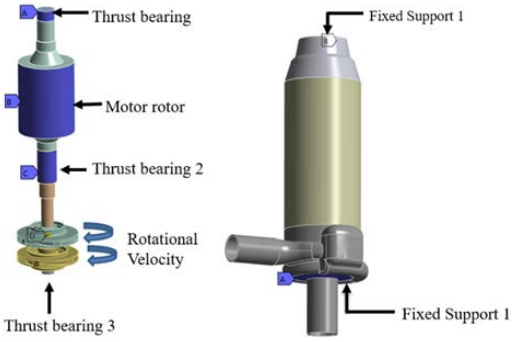

Figure 7: Boundary conditions of the pump model shaft and structural parts for FSI analysis

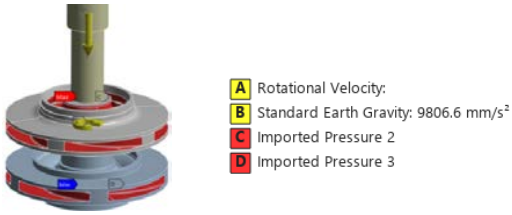

Figure 8: Boundary conditions of the pump impeller model for FSI analysis

The boundary conditions applied for the unidirectional FSI analysis are illustrated in **Figures 7** and **8 [15]**. In this approach, a three-dimensional steady-state CFD simulation is first performed to obtain the pressure distribution inside the pump flow passage. The pressure on the flow passage surface is then transferred to the surface of the structural domain of the centrifugal pump. In the case of the pump impeller, the fluid pressure obtained from CFD simulations was imported into the structural domain and applied at regions C and D (highlighted in red). The impeller rotational speed is N = 1731 min^{-1}, and the effect of gravity as an acceleration load with a value of 9.806 ms^{-2} was applied in the model.

4. Results and Discussion

4.1 Performance Curves of the Two-Stage Centrifugal Model

The performance curves of the two-stage centrifugal pump are shown in **Figure 9**. The pump efficiency at the best efficiency point (Q/Q_{BEP} =1.0) is 78%, which is comparatively lower than a pump of this kind [16], indicating a clear scope for hydraulic optimization in future designs, while Q/Q_{BEP}=0.8 at partial loading and Q/Q_{BEP}=1.2 at excessive loading conditions show lower efficiency values. As shown, the total head decreases gradually with the increase in flow rate, indicating typical pump behavior **[17][18].**

4.2 Internal Flow Characteristics

Figure 10 shows the pressure distributions in the pump flow passage of the 1st and 2nd stage pump flow passages, clearly illustrating the impact of varying flow rates on the system performance. At the best efficiency point of Q/Q_{BEP} = 1.0, the pump operates optimally, resulting in a uniform pressure distribution. Pressure distribution in the 2nd stage volute is more uniform compared to that of the partial flow rate condition of Q/Q_{BEP} = 0.8. At the excessive flow rate of Q/Q_{BEP} = 1.2, the overall pressure achieved in the second stage is comparatively lower than the

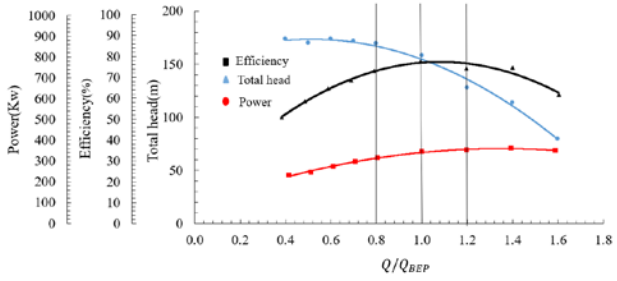

Figure 9: Performance curves of the two-stage centrifugal pump model

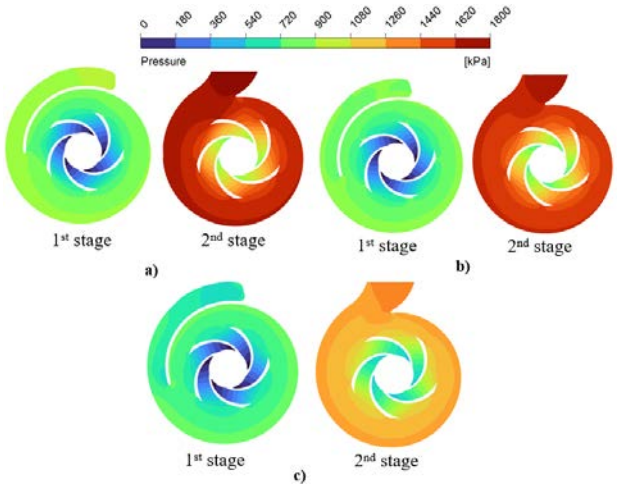

Figure 10: Static pressure distribution in two pump stages at a) Q/Q_{BEP} = 0.8, b) Q/Q_{BEP} = 1.0, and c) Q/Q_{BEP} = 1.2

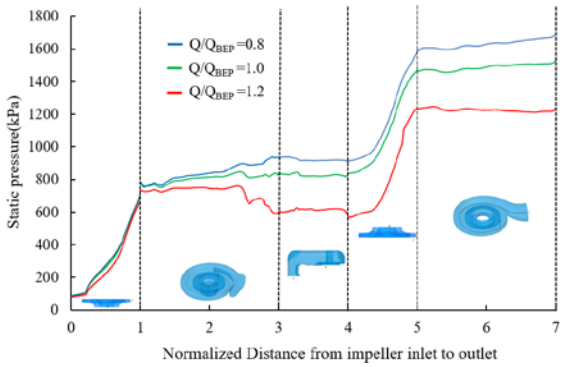

Figure 11: Pump pressure variation from the 1st stage to the 2nd stage

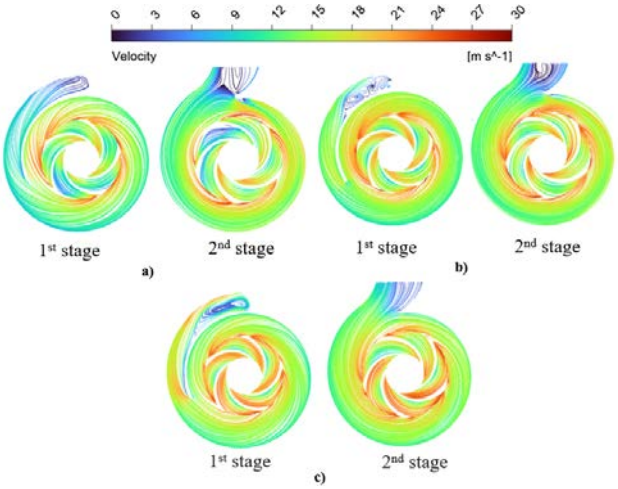

Figure 12: Streamline velocity distribution in two pump stages at a) Q/Q_{BEP} = 0.8, b) Q/Q_{BEP} = 1.0, and c) Q/Q_{BEP} = 1.2

pressures observed at the other flow rates. This reduction is primarily caused by a significantly higher pressure drop generated within the 1st stage volute casing at this high flow rate. This observation is strongly supported by the data presented in **Figure 11**, which confirms the substantial pressure loss occurring in the 1st stage volute casing (1 to 3 in **Figure 10**) in the flow path at the Q/Q_{BEP} = 1.2 condition, thereby limiting the pressure increase available for the subsequent second stage. This demonstrates how operating at an excessive flow rate introduces hydraulic losses for the pump operation.

Figure 11 shows the static pressure distributions in the two stages, revealing a consistent pressure rise across both the 1st and 2nd stage impellers. The 1st stage contributes less to the total pressure increment, accounting for about 45-41% depending on the flow rate, while the 2nd stage contributes around 49-45%. At the best efficiency point (Q/Q_{BEP} = 1), the pressure rise in the 1st stage is 45%, while in the 2nd stage it is 46%, indicating a more even pressure distribution between the two stages. At the excessive flow rate (Q/Q_{BEP} = 1.2), the 2nd stage develops a greater portion of the total pressure. This indicates that a balanced pressure development between stages is at the best efficiency point flow condition **[19].**

At the excessive flow rate condition of Q/Q_{BEP} = 1.2, the 1st stage volute casing shows a greater pressure drop compared with the other two flow rate conditions, causing a higher hydraulic loss. The velocity of streamlines increases as the flow rate increases **[20]**.

4.3 Total Head Loss Analysis

A numerical analysis of the internal flow can be employed to evaluate the hydraulic head loss in a pump **[21].**

$$h_{loss-rotating} = \frac{\frac{\tau\omega}{Q} - \Delta p_t}{\rho g H} \times 100\% \quad (1)$$

$$h_{loss-stationary} = \frac{\Delta p_t}{\rho g H} \times 100\% \quad (2)$$

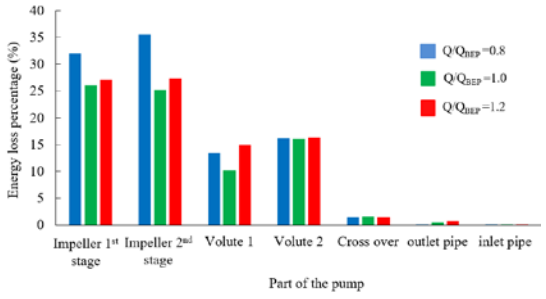

Figure 13: Total head loss percentage in the different parts of the pump model

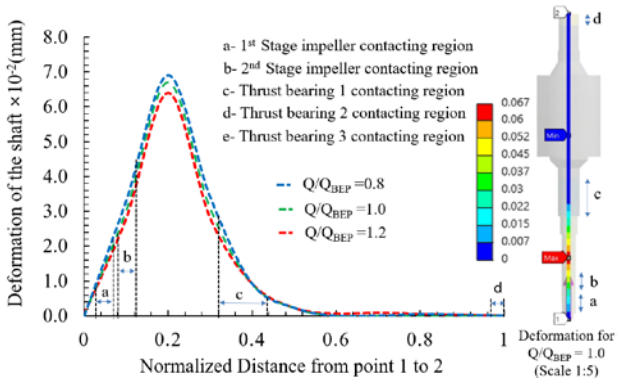

Figure 14: Deformation of the pump shaft along the shaft center-line

The total hydraulic head loss in the rotating part of the pump was calculated by using **Equation (1)**, and the other stationary parts, such as the volute casing, cross over, inlet, and outlet pipes, were calculated using **Equation (2)**. According to **Figure 13**, higher hydraulic loss can be seen in the rotating parts at the partial flow rate condition, but in the stationary parts of the pump flow passage, higher hydraulic loss is observed at the excessive flow rate condition **[12][21]**. The higher total head loss pressure drops, both at the rotating and stationary pump parts, cause a significant efficiency drop in the pump performance.

4.4 Structural Stability of the Pump Model

Pump shaft stability can be analyzed numerically using the FSI approach **[15]**. **Figure 14** shows the pump shaft deformation according to the variation of the flow rate. Unidirectional FSI analysis was carried out to evaluate the shaft deformation in the two-stage centrifugal pump model under three operating flow rate conditions: partial load (Q/Q_{BEP} = 0.8), best efficiency point (Q/Q_{BEP} = 1.0), and overload (Q/Q_{BEP} = 1.2). The results show that shaft deformation decreases with the increase in flow rate, reaching a maximum of 0.069 mm at the partial load condition. The contour plot in the scale of 1:5 indicates that the maximum deflection occurs above the contact region of the 2nd stage impeller. According to the API 610 and API 682 centrifugal pump standards **[23][24]**, the maximum allowable shaft deflection is 0.05 mm in places with bearings and seals, whereas the simulated results show that 9.3% of the area of the shaft is above this limit, which is outside the region covering bearings and seals. Hence, the shaft is acceptable with the given standards of API 610 and API 682.

Figure 15 shows that equivalent stress levels decrease with the increase of flow rate, reaching a maximum of about 21.8 MPa at the partial load (Q/Q_{BEP} = 0.8). The contour plot in the scale of 1:5 indicates that maximum stress concentration is located between regions

b and c, regardless of flow rate variation, whereas the region above c experiences minimal stress at the shaft measured along the center-line.

Figure 16 compares the equivalent stresses in key structural components of the two-stage pump at the best efficiency point (Q/Q_{BEP} = 1.0) using unidirectional FSI analysis. Results show that maximum stresses occur at localized regions of the impellers and shaft (highlighted in the red boxes) **[25][26]**. The 1st and 2nd stage impellers reach an equivalence stress level of 250 MPa and 280 MPa, respectively, both safely below their yield limits, while the shaft experiences a much lower stress of 81 MPa with a large safety margin. Further, based on the fatigue stress analysis **[27]** of the shaft and the two impellers. Based on S-N curves **[28][29]** for the relevant materials, the shaft material and impeller material have an endurance stress level that is less than the applied stress, considering loads to be applied periodically.

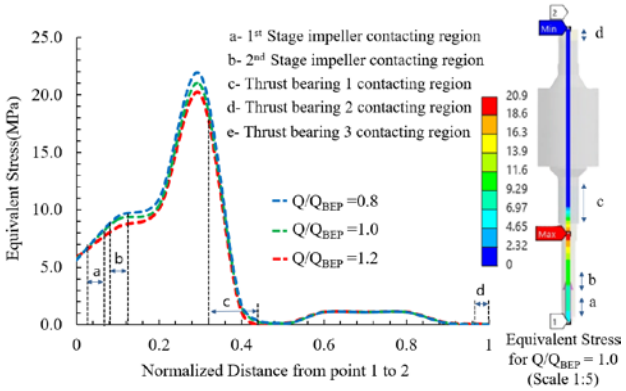

Figure 15: Equivalent stress of the pump shaft along the shaft center-line

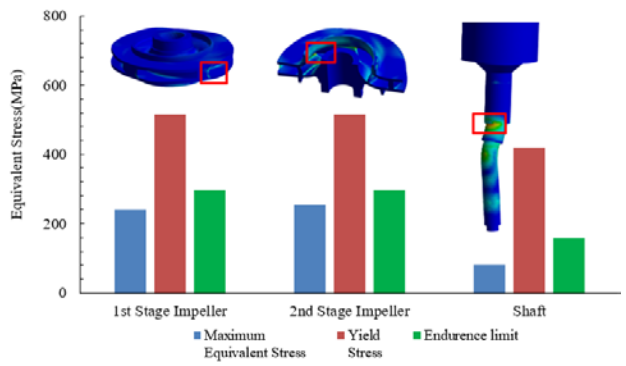

Figure 16: Comparison of yield stresses and endurance safety limits according to the components of the two-stage centrifugal pump for Q/Q_{BPE}=1.0, with each component deformed by a scale of 1:5

5. Conclusion

This study presented a numerical verification of the preliminary design of a high-head two-stage centrifugal pump model with a long shaft, combining CFD and FSI analyses to evaluate both hydraulic performance and structural stability. The CFD results indicated that the pump model achieved a maximum efficiency of 78% at the best efficiency point, although further design optimization is needed to approach the typical efficiency level of these types of pumps. Internal flow analysis shows a higher-pressure drop in 1st stage volute casing at the excessive flow rate condition, leading to a higher hydraulic loss. Further comparative higher hydraulic loss is observed in the impellers at the partial flow rate condition of Q/Q_{BEP} = 0.8. The unidirectional FSI analysis results revealed that the pump shaft remains structurally safe with respect to yield and endurance stresses. Though the shaft has a maximum shaft deflection of 0.069 mm in one localized region, it meets the industrial stability criteria of 0.05 mm given by API 610 and API 682 in the described locations for the shaft deformations.

Based on these results, future design optimization should focus on hydraulic performance, which can be improved by optimizing the 1st stage volute tongue geometry to reduce overload pressure drops.

Acknowledgement

This Research was supported (in part) by Glocal University Project of Mokpo National University in 2025.

Author Contributions

Conceptualization, E. Fernando, U. Shrestha, and Y. D. Choi; Methodology, E. Fernando; Software, E. Fernando; Validation, E. Fernando, U. Shrestha, and Y. D. Choi; Formal Analysis, E. Fernando; Investigation, E. Fernando; Resources, D. Kim; Writing—Original, E. Fernando; Writing—Review & Editing, Y. D. Choi; Supervision, Y. D. Choi; Funding Acquisition, Y. D. Choi.

References

[1] F. Fontana and M. Masi, “A hybrid experimental-numerical method to support the design of multistage pumps,” Energies, vol. 16, no. 12, p. 4637, 2023.

[2] H. Ding, W. Gao, and H. Gao, “CFD simulation of a multi-stage centrifugal pump,” Proceeding of the ASME 2017 Fluids Engineering Division Summer Meeting, p. FEDSM2017-69587, 2017.

[3] M. M. Shamsuddeen, S. Kim, M. A. Shahzer, S. -B. Ma, and J. -H. Kim, "Numerical investigation of losses in a double-suction multistage centrifugal pump and its mitigation using baffle plates," Frontiers in Energy Research, vol. 10, p. 969706, 2022.

[4] Y. D. Choi, "Investigation on the internal flow characteristics of the low specific speed centrifugal pump with circular casing," Journal of the Korean Society of Marine Engineering, vol. 32, no. 3, pp. 404-412, 2008.

[5] S. Yan, Z. Ye, D. Wang, J. Ma, and W. Zhou, "Structural analysis and optimization of ultra-high-speed centrifugal pump rotor system considering fluid–structure interaction," Water, vol. 16, no. 11, p. 1471, 2024.

[6] L. Yadeta, H. G. Lemu, and A. Tadese, "Fluid structure interaction induced fatigue stress analysis of multi-stage centrifugal water pump shaft under varying load condition," Journal of the Brazilian Society of Mechanical Sciences and Engineering, vol. 47, no. 8, p. 395, 2025.

[7] B. Mischo, P. Jenny, S. Mauri, Y. Bidaut, M. Kramer, and S. Spengler, "Numerical and experimental fluid–structure interaction-study to determine mechanical stresses induced by rotating stall in unshrouded centrifugal compressor impellers," Journal of Turbomachinery, vol. 140, no. 11, p. 111006, 2018.

[8] A. Albadawi, M. Specklin, R. Connolly, and Y. Delauré, "A thin film fluid structure interaction model for the study of flexible structure dynamics in centrifugal pumps," Journal of Fluids Engineering, vol. 141, no. 6, p. 061402, 2018.

[9] W. Zhou, J. Ma, Z. Ma, W. Yu, H. Su, and B. Gao, "Fluid–structure interaction on the rotor-dynamic characteristics of a low-specific-speed centrifugal pump considering multi-scale fluid excitation effects," Physics of Fluids, vol. 36, no. 11, p. 117157, 2024.

[10] ANSYS Inc., 2025, ANSYS documentation ver. 2025R1, http://www.ansys.com, Accessed July 25th, 2025.

[11] Y. Long, B. Lin, J. Fang, J. Ge, L. Xu, Q. Fu, and R. Zhu, "Research on the pump shaft stability analysis of multistage centrifugal pump during closed-valve start-up process," Frontiers in Energy Research, vol. 8, p. 186, 2020.

[12] C. Wang, W. Shi, X. Wang, X. Jiang, Y. Yang, W. Li, and L. Zhou, "Optimal design of multistage centrifugal pump based on the combined energy loss model and computational fluid dynamics," Applied Energy, vol. 187, pp. 10-26, 2017.

[13] T. Xin, J. Wei, L. Qiuying, G. Hou, Z. Ning, W. Yuchuan, and C. Diyi, "Analysis of hydraulic loss of the centrifugal pump as turbine based on internal flow feature and entropy generation theory," Sustainable Energy Technologies and Assessments, vol. 52, p. 102070, 2022.

[14] T. P. Dhakal and D. K. Walters, "A three-equation variant of the SST k-ω model sensitized to rotation and curvature effects," Journal of Fluids Engineering, vol. 133, no. 11, p. 111201, 2011.

[15] S. Li, Y. Tu, C. Ye, H. Yan, J. Dai, M. Dang, C. Yang, Y. Zheng, and Y. Li, "Analysis of stress characteristics of a vertical centrifugal pump based on fluid-structure interaction," Water, vol. 15, no. 24, p. 4269, 2023.

[16] D. Zhu, Z. Hu, Y. Chen, C. Wang, Y. Yang, J. Lu, X. Song, R. Tao, Z. Wang, and W. Ma, "Improvement design of a two-stage double-suction centrifugal pump for wide-range efficiency enhancement," Water, vol. 15, no. 9, p. 1785, 2023.

[17] M. Guo, Z. Chen, and Y. -D. Choi, "Design and CFD analysis of screw centrifugal pump model," Journal of the Korean Society of Marine Engineering, vol. 43, no. 8, pp. 640-647, 2019.

[18] J. O. Mo, Y. T. Kim, and Y. H. Lee, "Numerical study on cavitation performance evaluation in a centrifugal pump impeller," Journal of the Korean Society of Marine Engineering, vol. 36, no. 2, pp. 286–293, 2012.

[19] R. Xue, X. Lin, B. Zhang, H. Zhou, T. Lai, and Y. Hou, "CFD and energy loss model analysis of high-speed centrifugal pump with low specific speed," Applied Sciences, vol. 12, no. 15, p. 7435, 2022.

[20] W. Wang, Q. Deng, J. Pei, J. Chen, and X. Gan, "Discrete optimization on unsteady pressure fluctuation of a centrifugal pump using ANN and modified GA," Chinese Journal of Mechanical Engineering, vol. 36, no. 1, p. 84, 2023.

[21] Y. Zhang, S. Hu, Y. Zhang, and L. Chen, "Optimization and analysis of centrifugal pump considering fluid-structure interaction," The Scientific World Journal, vol. 2014, p. 131802, 2014.

[22] A. J. Stepanoff, Centrifugal and Axial Flow Pumps: Theory, Design, and Application, 2nd edition, New York, USA: John Wiley & Sons, Inc, 1957.

[23] American Petroleum Institute: Centrifugal Pumps for Petroleum, Petrochemical and Natural Gas Industries, API

Standard 610, 12th ed., American Petroleum Institute, Washington, DC, USA, Jan. 2021.

[24] American Petroleum Institute: Pumps- Shaft sealings for centrifugal and Rotary Pumps, API Standard 682, 4th ed., American Petroleum Institute, Washington, DC, USA, May. 2014.

[25] J. Yuan, J. Shi, Y. Fu, H. Chen, R. Lu, and X. Hou, “Analysis of fluid-structure coupling dynamic characteristics of centrifugal pump rotor system,” Energies, vol. 15, no. 6, p. 2133, 2022.

[26] J. R. Cho, J. M. Song, and J. K. Lee, “Finite element techniques for the free-vibration and seismic analysis of liquid-storage tanks,” Finite Elements in Analysis and Design, vol. 37, no. 6–7, pp. 467–483, 2001.

[27] D. B. Marghitu, C. I. Diaconescu, and B. O. Ciocirlan, “Mechanics of Materials,” in Mechanical Engineer’s Handbook. San Diego, CA, USA: Academic Press, ch. 3, pp. 119–188, 2001.

[28] JAHM Software, Inc., "Temperature Dependent Material Properties Database (MPDB)," JAHM.com, North Reading, MA, USA, 2025.

[29] Q. Fu, D. Wang, R. Zhang, Y. Lu, R. Wang, and R. Zhu, “Stress analysis and stress fatigue life prediction of RCP impeller based on fluid-thermal-solid coupling,” Nuclear Engineering and Design, vol. 414, p. 112596, 2023.